A Novel Method for Characterization of Peripheral Nerve Fiber Size Distributions by Group Delay

Robert B. Szlavik*

***Abstract*—The ability to determine the characteristics of peripheral nerve fiber size distributions would provide additional information to clinicians for the diagnosis of specific pathologies of the peripheral nervous system. Investigation of these conditions, using electrodiagnostic techniques, is advantageous in the sense that such techniques tend to be minimally invasive yet provide valuable diagnostic information. One of the principal electrodiagnostic tools available to the clinician is the nerve conduction velocity test. While the peripheral nerve conduction velocity test can provide useful information to the clinician regarding the viability of the nerve under study, it is a single-parameter test that yields no detailed information about the characteristics of the functioning nerve fibers within the nerve trunk. In this study, we present a technique based on decomposition of the maximal compound evoked potential and subsequent determination of the group delay of the contributing nerve fibers. The fiber group delay is then utilized as an initial estimation of the nerve fiber size distribution and the associated temporal propagation delays of the single-fiber-evoked potentials to a reference electrode. Simulation studies, based on deterministic single-fiber action potential functions, are used to demonstrate the robustness of the proposed technique in the presence of simulated noise associated with the recording process.**

***Index Terms*—Conduction velocity distribution (CVD), group delay, nerve fiber size distribution.**

I. Introduction

The nerve conduction velocity test provides clinically useful information in the diagnosis of peripheral neuropathies, such as carpal tunnel syndrome [1], [2]. Since nerve conduction velocity studies are essentially single parameter measurements of the gross conduction properties of the underlying nerve trunk, such studies are not suited to providing detailed information regarding the characteristics of the underlying nerve fibers that contribute to the compound evoked potential.

A more robust measurement technique would involve the ability to extract information about the population of nerve fibers within the nerve trunk that are contributing to the evoked potential that could potentially provide useful information to the clinician. As an example, information related to the size distribution of contributing nerve fibers can be used to differentiate between different clinical conditions such as chronic inflammatory demyelinating polyneuropathy, which selectively impacts larger nerve fibers, or early diabetic peripheral neuropathy, which impacts smaller fibers [3], [4].

There is a large body of literature devoted to describing various techniques for determining the nerve fiber conduction velocity distribution (CVD). The pioneering work of Cummins *et al.* [5] and Dorfman [6] describe techniques that use two compound action potentials to estimate the CVD using a least squares approach. Common to these studies was the assumption that fibers included in a specific velocity class have identical evoked potentials waveforms.

More recently, there have been several additional studies including the work of Gonzalez-Cueto and Parker [7], Papadopoulou and Panas [8], and Gu *et al.* [9]. The studies presented by Tu *et al.* and Morita *et al.* focused on a regularized least squares algorithm but feature many of the same assumptions associated with waveform commonality related to velocity classes that were made in earlier work [10], [11]. This study also investigated the impact of recording noise on the integrity of the estimated CVD. Bayramoglu *et al.* investigated the distribution of peroneal nerve conduction velocities using a collision technique [12].

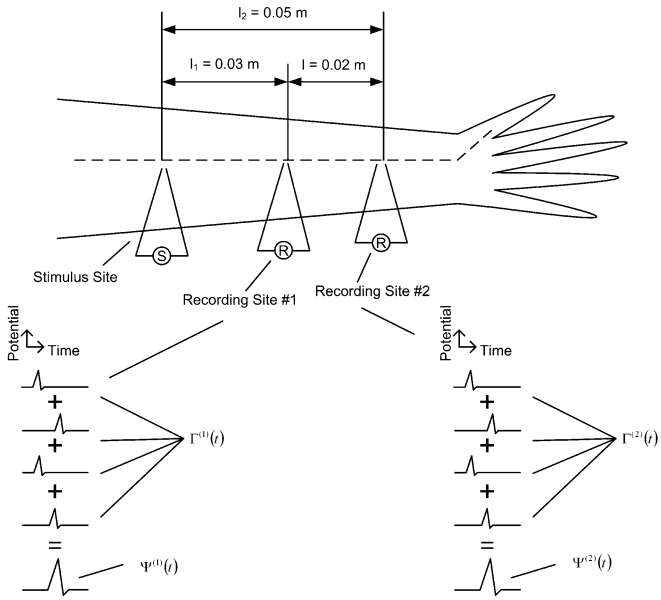

Fig. 1. Conceptual physical configuration of the proposed method. The diagram shows the stimulus and recording sites as well as the relationship between the individual single-fiber-evoked potentials sets $\mathbf{\Gamma^{(1)}}(t)$ and $\mathbf{\Gamma^{(2)}}(t)$ to the maximal compound evoked potentials $\Psi^{(1)}(t)$ and $\Psi^{(2)}(t)$. The figure is not drawn to scale and is indicative of stimulation and recording sites at convenient locations along the median nerve. From an experimental perspective, implementation could involve stimulation of the median nerve at the anterior cubital fossa with recording sites placed more distally at anatomically convenient locations such as the wrist. This type of placement would result in distances that are larger than those indicated on the figure.

In this paper, we present a novel technique for estimating the size distribution of contributing nerve fibers that is linearly related to the CVD. The technique is based on an estimation of the group delay between two sets of recording electrodes associated with the individual fibers that contribute to a maximal compound-evoked potential. The group delay information is then used to estimate the diameters of the activated fibers as well as the propagation delays of individual single-fiber-evoked potentials to a reference electrode. This process allows for reconstruction of an estimated maximal compound evoked potential, from the individual single-fiber-evoked potentials, at the first recording site.

The basic methodology behind the technique is presented by utilizing a closed-form mathematical model of a single-fiber-evoked potential waveform that allows us to demonstrate the robustness of the technique under noisy conditions.

II. Method

The simulation for determination of the group delay is premised on the physical setup shown in Fig. 1, where a stimulator is used to excite a subcutaneous nerve trunk consisting of a group of electrically independent nerve fibers. While the dimensions of the distance between the stimulus and recording electrodes were chosen for simulation convenience, an experimental implementation of the study could

Manuscript received August 2, 2007; revised December 14, 2007. Current version published December 17, 2008. *Asterisk indicates corresponding author*.

*R. B. Szlavik is with the Department of Biomedical and General Engineering, California Polytechnic State University, San Luis Obispo, CA 93407-0350 USA (e-mail: rszlavik@calpoly.edu).

Color versions of one or more of the figures in this paper are available online at http://ieeexplore.org.

Digital Object Identifier 10.1109/TBME.2008.921149

be made with the stimulus site at the anterior cubital fossa for stimulation of the median nerve. Recording electrodes could be placed more distally along the course of the median nerve. The propagating compound-evoked potential is detected at two recording sites. Using a series of successively increasing current stimulus pulses, the successively recorded compound evoked potentials can be decomposed into their constituent single fiber action potentials in a manner analogous to the protocol used in the McComas *et al.* motor unit number estimation technique [13].

There are several assumptions that are inherent to the simulation study presented in this paper that have been made by other investigators [9], [14]. When stimulated, it is assumed that each active nerve fiber transmits the single fiber action potential at the same time from the site of the stimulating electrode. While it is acknowledged that there is evidence that the threshold required to excite a nerve fiber is not a precise value but fluctuates over a small range, this study assumes a fixed value of stimulus current, dependent on nerve fiber size, for fiber recruitment [15]. It is further assumed that the CVD is invariant along the nerve although there is some evidence to the contrary [16]. A linear relationship between conduction velocity and fiber diameter is also assumed [17], although there is some evidence that pathological conditions, such as disruption of the myelin, can result in this relationship becoming nonlinear [18]. It is acknowledged that nerve fiber depth will influence activation characteristics at a given stimulus current level as will tissue anisotropy [19]. These effects are not typically included in techniques that have been proposed for determining the nerve fiber size or CVDs and are not included in this proposed technique [9], [10].

A. Generation of Compound Action Potential Waveforms, Single Fiber Action Potential Decomposition, and Group Delay Estimation

An empirically determined nerve fiber diameter distribution [20] was used to generate a random population of 100 nerve fiber diameters for two distributions using a technique described by Szlavik and de Bruin [21]. The distribution in (1) was used to generate the fiber diameter population:

$$p_d(d_k) = \sum_{h=1}^{4} \frac{\beta_h}{\sigma_h \sqrt{2\pi}} \exp\left[-\frac{(d_k - \mu_h)^2}{2\sigma_h^2}\right]. \tag{1}$$

The parameters shown in Table I were used in the distribution of (1).

The randomly generated fiber diameter distributions formed the template distribution population $\boldsymbol{d}$.

The population of nerve fibers in each distribution was subjected to a series of virtual stimulus pulses of successively increasing current amplitude where Ω_i is the amplitude of the stimulus current pulse at each increment i. An activation function $\xi(d)$ was used to determine whether a given stimulus current amplitude was sufficient to excite each fiber with diameter d as per (2) where $\zeta = 10\,\mathrm{mA}$ and $\eta = 3.5 \times 10^5\ \mathrm{m}^{-1}$:

$$\xi(d) = \zeta \exp[-\eta d]. \tag{2}$$

For each recording site $n = 1, 2$, the compound evoked potential $\Psi_i^{(n)}(t)$ is computed for each increment i of the stimulus current amplitude as per

$$\Psi_i^{(n)}(t) = \sum_{k=1}^{m} u[\Omega_i - \xi(d_k)] G[v_k \cdot (t - \delta_k^{(n)}), \bar{r}]. \tag{3}$$

In (3), the single fiber action potential waveform $G[v_k(t - \delta_k^{(n)}), \bar{r}]$ contributes to the compound-evoked potential if the argument of the step function u is positive where t is the time in seconds, v_k is the conduction velocity of the kth fiber, $\delta_k^{(n)}$ is the propagation delay (in seconds) of the single fiber action potential from the stimulus site to the nth recording site, and $\bar{r}$ is the perpendicular depth between the recording site and the center of the kth fiber.

TABLE I
PARAMETER VALUES USED IN THE FIBER DIAMETER DISTRIBUTION

Symbol	Quantity	Value
β_1	complete distribution 1st mode scaling const.	0.05 (m)
σ_1	complete distribution 1st mode std. dev.	0.1274 (μm)
μ_1	complete distribution 1st mode mean	0.5 (μm)
β_2	complete distribution 2nd mode scaling const	0.25 (m)
σ_2	complete distribution 2nd mode std. dev.	0.8493 (μm)
μ_2	complete distribution 2nd mode mean	3 (μm)
β_3	complete distribution 3rd mode scaling const.	0.3 (m)
σ_3	complete distribution 3rd mode std. dev.	1.699 (μm)
μ_3	complete distribution 3rd mode mean	7.5 (μm)
β_4	complete distribution 4th mode scaling const.	0.4 (m)
σ_4	complete distribution 4th mode std. dev.	1.699 (μm)
μ_4	complete distribution 4th mode mean	13 (μm)
β_1	large distribution 1st mode scaling const.	0.3 (m)
σ_1	large distribution 1st mode std. dev.	1.699 (μm)
μ_1	large distribution 1st mode mean	7.5 (μm)
β_2	large distribution 2nd mode scaling const	0.7 (m)
σ_2	large distribution 2nd mode std. dev.	1.699 (μm)
μ_2	large distribution 2nd mode mean	13 (μm)
β_3	large distribution 3rd mode scaling const.	0 (m)
σ_3	large distribution 3rd mode std. dev.	-
μ_3	large distribution 3rd mode mean	-
β_4	large distribution 4th mode scaling const.	0 (m)
σ_4	large distribution 4th mode std. dev.	-
μ_4	large distribution 4th mode mean	-

The function G is the model of the single fiber action potential proposed by Fleisher *et al.* where the function has been normalized to the current through the second pole such that $G = g/I$, as per (4). All other parameters are as described Fleisher [22] and were assigned values $a_k = d_k/2$, $s_k = 5 \cdot a_k$, $\bar{r} = 1\,\mathrm{mm}$, $v_k = c \cdot d_k$, $\alpha = 0.75$, and $\sigma_e = 1.0\,\mathrm{S/m}$, $D_k = (a_k + s_k)/(\bar{r} + s_k)$, $u_k = s_k(1 + \alpha)/(1 - \alpha)$:

$$\begin{aligned} &G[v_k \cdot (t - \delta_k^{(n)}), \bar{r}] \\ &= \frac{D_k^2}{4\pi\sigma_e a_k}\left[\alpha \exp\left\{-\left(\frac{D_k}{4}\right)^2\left(\frac{v_k \cdot (t - \delta_k^{(n)}) + s_k}{a_k}\right)^2\right\}\right. \\ &\quad -\exp\left\{-\left(\frac{D_k}{4}\right)^2\left(\frac{v_k \cdot (t - \delta_k^{(n)}) - s_k}{a_k}\right)^2\right\} \\ &\quad \left.+(1-\alpha)\exp\left\{-\left(\frac{D_k}{4}\right)^2\left(\frac{v_k \cdot (t - \delta_k^{(n)}) - u_k}{a_k}\right)^2\right\}\right]. \end{aligned} \tag{4}$$

After the compound-evoked potentials are computed for each virtual current step Ω_i, the series of compound-evoked potentials at each recording site $\boldsymbol{\Psi}^{(1)}(\mathbf{t})$ and $\boldsymbol{\Psi}^{(2)}(\mathbf{t})$ are decomposed into a series of waveforms that nominally consist of the contributing single fiber action potentials at each simulated current step $\boldsymbol{\Gamma}^{(1)}(\mathbf{t})$ and $\boldsymbol{\Gamma}^{(2)}(\mathbf{t})$ as

$$\Gamma_{i-1}^{(n)}(t) = \Psi_i^{(n)}(t) - \Psi_{i-1}^{(n)}(t) \qquad \text{for } 2 \le i \le q + 1. \tag{5}$$

If the current steps are small enough, then the waveforms $\boldsymbol{\Gamma}^{(\mathbf{n})}(\mathbf{t})$ will consist of individual contributing single fiber action potentials or no waveform where a stimulus current increment does not result in an additional recruited fiber. However, a perfect decomposition will not always be achievable due to the finite discretization of the stimulus

current steps. Some of the q nonzero waveforms in the set $\mathbf{\Gamma^{(n)}(t)}$ will consist of more than one single fiber action potential.

Once the decomposition is complete, the individual decomposed waveforms from the two recording sites can be used to compute an estimate of the group delay associated with each contributing nerve fiber where the frequency response of a given fiber $H_{i-1}(f)$ is as shown in (6):

$$H_{i-1}(f) = \frac{\Im[\Gamma_{i-1}^{(2)}(t)]}{\Im[\Gamma_{i-1}^{(1)}(t)]}. \tag{6}$$

The frequency response is computed by dividing the Fourier transform of the single-fiber-evoked potential associated with the more distal recording site by the Fourier transform of the single-fiber-evoked potential associated with the more proximal recording site. Since each $H_{i-1}(f) = |H_{i-1}(f)|\angle\Theta_{i-1}(f)$, an estimate of the group delay τ_{i-1} for each pair of nonzero decomposed waveforms $\Gamma_{i-1}^{(1)}(t)$ and $\Gamma_{i-1}^{(2)}(t)$ can be computed from (7):

$$\tau_{i-1} = -\frac{1}{2\pi}\frac{d\Theta_{i-1}(f)}{df}. \tag{7}$$

In practice, a least squares line is fitted to the phase response $\Theta_{i-1}(f)$ for the $H_{i-1}(f)$ computed for each pair of nonzero decomposed waveforms $\Gamma_{i-1}^{(1)}(t)$ and $\Gamma_{i-1}^{(2)}(t)$, which facilitates the computation of the associated group delay τ_{i-1}. The estimated group delays for the contributing nerve fibers are used to compute an estimate of the associated fiber diameters from (8) where *l*(*m*) is the distance between the two recording sites and $c = 5.0 \times 10^5 s^{-1}$.

$$d_{i-1} = \frac{l}{c\tau_{i-1}}. \tag{8}$$

Once the estimated group delay is computed for each nonzero pair of decomposed waveforms $\Gamma_{i-1}^{(1)}(t)$ and $\Gamma_{i-1}^{(2)}(t)$, an estimate of the sequence of nerve fiber diameters $\tilde{\mathbf{d}}$ is obtained for the contributing fiber population.

The overall process described before is illustrated in the flowchart of Fig. 2.

To more realistically evaluate the efficacy of the proposed method, recording noise effects were studied. The set of decomposed single fiber evoked potentials at each electrode were assumed to be corrupted by recording noise $n(t)$ that was assumed to be Gaussian distributed such that $\Gamma_{i-1}^{(n)}(t) = \Psi_i^{(n)}(t) - \Psi_{i-1}^{(n)}(t) + n(t)$ for $2 \le i \le q+1$. The average SNR for the population is defined in terms of the average of the mean signal power for all the single fiber action potentials in the population and the Gaussian distributed noise power.

III. Results

Two populations of 100 randomly generated fibers from the complete and large fiber distributions were utilized in these studies. For the complete distribution, fibers with diameters less than 5 μm were rejected. In the case of the large distribution, fibers falling between 2 μm and 10 μm were accepted. The fibers from each distribution were subjected to a virtual stimulus pulse train of successively increasing amplitudes ranging from zero to a maximum of 1 mA in 500 nA steps. At each step the compound evoked potential at both virtual recording sites was computed as per (3), and subsequently, the estimate of single fiber action potential waveforms were obtained at each recording site as per (5). The concomitant group delays between the two virtual recording sites were computed yielding the group delay estimated set of fiber diameters $\tilde{\mathbf{d}}$.

A histogram comparing the actual template fiber population $\mathbf{d}$ to the group delay estimated population $\tilde{\mathbf{d}}$ is shown in Fig. 3.

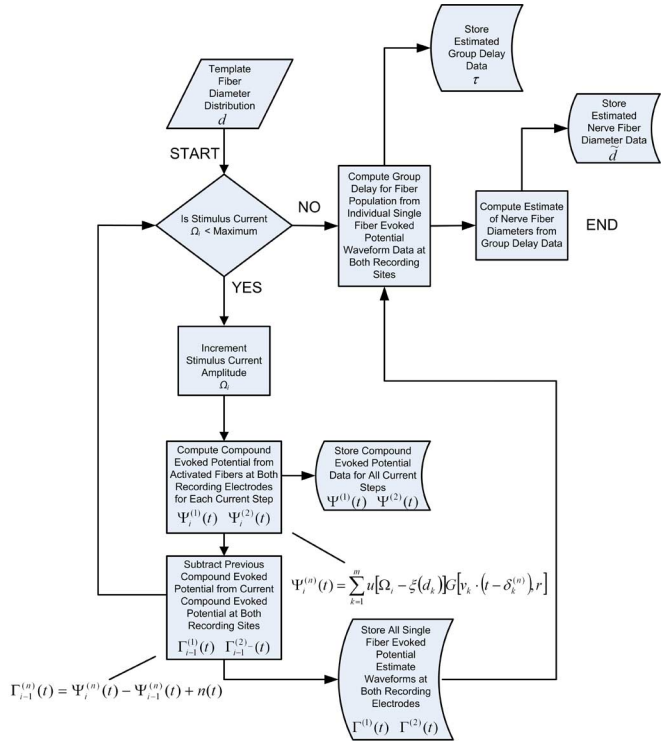

Fig. 2. Flowchart of the algorithm implemented to calculate an estimate of the group delay of the contributing population of nerve fibers and the estimated fiber diameter set $\tilde{\mathbf{d}}$. The technique is based on determination of an estimate of the group delay associated with each nonzero decomposed waveform $\Gamma_{i-1}^{(1)}(t)$ and $\Gamma_{i-1}^{(2)}(t)$.

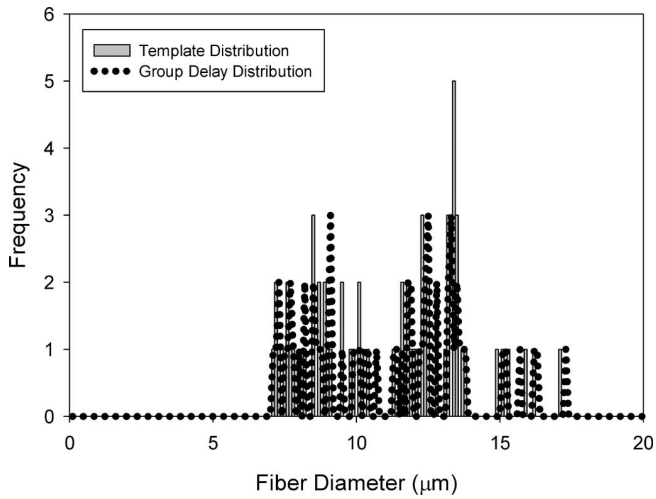

Fig. 3. Histogram of the template nerve fiber size population $\boldsymbol{d}$ from the complete fiber distribution and group delay estimated nerve fiber size population $\tilde{\boldsymbol{d}}$ for the no noise case. The normalized final error, as defined in (9), is FE = 58.4831% and the chi-square test results for the two distributions yielded $Q(\chi^2\,|x) = 0.9791$.

Fig. 4 compares the maximal template compound evoked potential at the first electrode $\Psi_{q+1}^{(1)}(t)$ with the maximal group delay estimated compound evoked potential $\tilde{\Psi}_{q+1}^{(1)}(t)$ for the distributions shown in Fig. 3.

The effect of the impact of recording noise was also studied. Fig. 5 is a plot of the chi-square test and FE results over the range of the SNR values investigated.

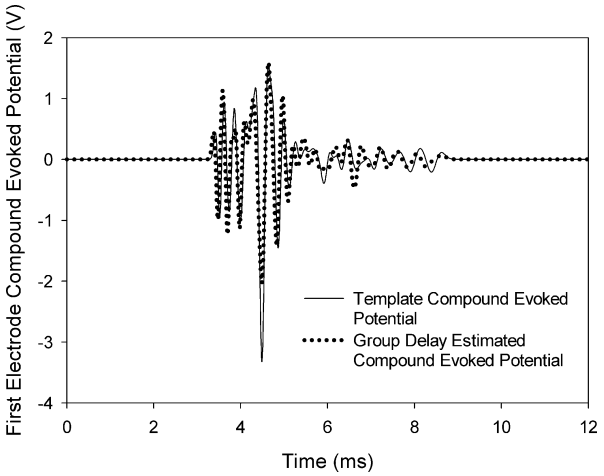

Fig. 4. Graph comparing the template maximal compound evoked potential of the complete fiber distribution to the group delay estimated maximal compound evoked potential for the no noise case. The graph shows the template maximal compound evoked potential at the first recording site $\Psi_{q+1}^{(1)}(t)$ and the group delay estimated maximal compound evoked potential at the first recording site $\tilde{\Psi}_{q+1}^{(1)}(t)$. The normalized final error, as defined in (9), is FE $= 58.4831\%$ and the chi-squared test result is $Q(\chi^2\,|x) = 0.9791$.

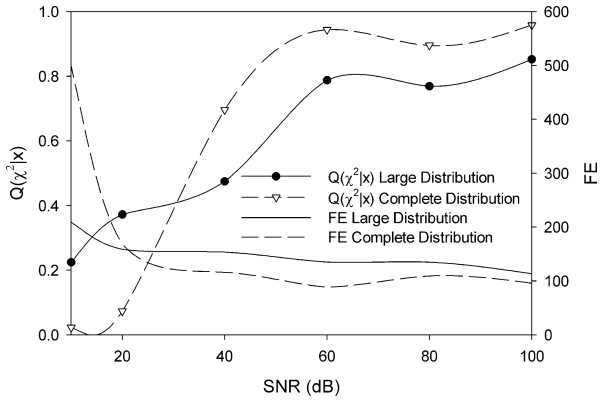

Fig. 5. Chi-square test results and final normalized error FE for different values of SNR for the complete and large fiber distributions. The plot shows the averaged results for three runs at different SNR levels.

The normalized final error *FE*, referred to in the previous figures, was calculated as per (9).

$$FE = \left(\frac{\left\| \Psi^{(1)}(t) - \tilde{\Psi}^{(1)}(t) \right\|_2}{\left\| \Psi^{(1)}(t) \right\|_2} \right) \times 100\%. \tag{9}$$

IV. Discussion

The results of the simulation study presented earlier demonstrate that the technique presented herein can, with reasonable accuracy, retrieve the fiber size distribution in the presence of recording noise for a wide range of SNR values.

The graph shown in Fig. 5 further demonstrates relatively low *FE* values for SNR values of 20 dB or larger. While *FE* provides a quantitative assessment of the fidelity with which the group delay estimated distribution compound evoked potential reproduces the template or actual compound evoked potential, the chi-square test provides a quantitative assessment of the fidelity with which the template distribution is estimated by the group delay process. The group delay estimator performance is seriously impacted for SNR levels below 20 dB. At lower SNR levels the estimated slopes of the phase spectra associated with the frequency response of the individual fibers are no longer accurate enough for a high fidelity reproduction of the template distribution or the temporal waveform of the compound evoked potential.

The proposed technique for measuring the size distribution of nerve fibers that contribute to the maximal compound evoked potential has several advantages over other earlier proposed methods. Unlike some previous techniques [5], [10], no inherent assumptions are made regarding size based classification of contributing single fiber evoked potentials. Each contributing single fiber evoked potential can, in theory, have a unique wave shape. The fact that many of the other techniques stipulate specific forms of the single fiber action potential waveforms, based upon dividing the range of fiber diameters into distinct groups, makes direct comparison with these techniques problematic.

One of the disadvantages of the proposed approach, in comparison to other techniques, is the necessity to perform a series of compound evoked potential measurements associated with a train of successively increasing stimulus current pulse amplitudes. While the measurement associated with the proposed method is more involved, the protocols for extracting individual contributing evoked potentials based upon a successively increasing stimulus pulse amplitude is well established in the literature on motor unit number estimation [13].

References

[1] P. A. Parker and P. Kelly, "Nerve conduction velocity measurement techniques," *J. Clin. Eng.*, vol. 7, no. 2, pp. 153–158, Apr. 1982.

[2] I. Atroshi, C. Gummesson, R. Johnsson, and E. Ornstein, "Diagnostic properties of nerve conduction tests in population-based carpal tunnel syndrome," *BMC Musculoskeletal Disord.*, vol. 4, no. 1, p. 9, May 2003.

[3] Y. Harati, "Diabetic peripheral neuropathies," *Ann. Intern. Med.*, vol. 107, pp. 546–559, 1987.

[4] L. J. Dorfman, K. L. Cummins, G. M. Reaven, J. Ceranski, M. S. Greenfield, and L. Doberne, "Studies of diabetic polyneuropathy using conduction velocity distribution (DCV) analysis," *Neurology*, vol. 33, no. 6, pp. 773–779, Jun. 1983.

[5] K. L. Cummins, L. J. Dorfman, and D. H. Perkel, "Nerve fiber conduction–velocity distributions—II. Estimation based on two compound action potentials," *Electroencephalogr. Clin. Neurophysiol.*, vol. 46, no. 6, pp. 647–658, 1979.

[6] L. J. Dorfman, "The distribution of conduction velocities (DCV) in peripheral nerves: A review," *Muscle Nerve*, vol. 7, no. 1, pp. 2–11, 1984.

[7] J. A. Gonzalez-Cueto and P. A. Parker, "Deconvolution estimation of nerve conduction velocity distribution," *IEEE Trans. Biomed. Eng.*, vol. 49, no. 2, pp. 140–151, Feb. 2002.

[8] F. A. Papadopoulou and S. M. Panas, "Estimation of the nerve conduction velocity distribution by peeling sampled compound action potentials," *IEEE Trans. Magn.*, vol. 35, no. 3, pp. 1801–1804, May 1999.

[9] D. Gu, R. E. Gander, and E. C. Crichlow, "Determination of nerve conduction velocity distribution from sampled compound action potential signals," *IEEE Trans. Biomed. Eng.*, vol. 43, no. 8, pp. 829–838, Aug. 1996.

[10] Y. X. Tu, A. Wernsdorfer, S. Honda, and Y. Tomita, "Estimation of conduction velocity distribution by regularized-least-squares method," *IEEE Trans. Biomed. Eng.*, vol. 44, no. 11, pp. 1102–1106, Nov. 1997.

[11] G. Morita, Y. X. Tu, Y. Okajima, S. Honda, and Y. Tomita, "Estimation of the conduction velocity distribution of human sensory nerve fibers," *J. Electromyogr. Kinesiol.*, vol. 12, pp. 37–43, 2002.

[12] F. G. Bayramoglu, N. Dalkilic, E. Kiziltan, and I. Demirel, "Deep peroneal motor nerve conduction velocity distribution and correlation between nerve conduction groups and the number of innervated muscle fibers," *Int. J. Neurosci.*, vol. 114, pp. 1147–1159, Sep. 2004.

[13] A. J. McComas, P. R. W. Fawcett, M. J. Campbell, and R. E. P. Sica, "Electrophysiological estimation of the number of motor units within a human muscle," *J. Neurol. Neurosurg., Psychiatry*, vol. 34, pp. 121–131, 1971.

[14] G. Hirose, Y. Tsuchitani, and J. Huang, "A new method for estimation of nerve conduction velocity distribution in the frequency domain," *Electroencephalogr. Clin. Neurophysiol.*, vol. 63, pp. 192–202, 1986.

[15] P. G. Ridall, A. N. Pettitt, R. D. Henderson, and P. A. McCombe, "Motor unit number estimation—a Bayesian approach," *Biometrics*, vol. 62, pp. 1235–1250, Dec. 2006.
[16] F. Pehlivan, N. Dalkilic, and E. Kiziltan, "Does the conduction velocity distribution change along the nerve," *Med. Eng. Phys.*, vol. 26, pp. 395–401, 2004.
[17] J. Erlanger and H. S. Gasser, *Electrical Signs of Nervous Activity*. Philadelphia, PA: Univ. of Pennsylvania Press, 1937.
[18] S. Reutskiy, E. Rossoni, and B. Tirozzi, "Conduction in bundles of demyelinated nerve fibers: Computer simulation," *Biol. Cybern.*, vol. 89, pp. 439–448, 2003.
[19] R. B. Szlavik and H. de Bruin, "The effect of anisotropy on the potential distribution in biological tissue and its impact on nerve excitation simulations," *IEEE Trans. Biomed. Eng.*, vol. 47, no. 9, pp. 1202–1210, Sep. 2000.
[20] I. A. Boyd and M. R. Davey, *Composition of Peripheral Nerves*. Edinburgh, U.K.: E & S Livingstone, 1968.
[21] R. B. Szlavik and H. de Bruin, "Simulating the distribution of axon size in nerves," in *Proc. 23rd Can. Med. Biol. Eng. Soc.*, 1997, pp. 168–169.
[22] S. M. Fleisher, M. Studer, and G. S. Moschytz, "Mathematical model of the single-fiber action potential," *Med. Biol. Eng. Comput.*, vol. 22, pp. 433–439, 1984.

Measuring Saccade Peak Velocity Using a Low-Frequency Sampling Rate of 50 Hz

Roel Wierts, Maurice J. A. Janssen*, and Herman Kingma

***Abstract*—During the last decades, small head-mounted video eye trackers have been developed in order to record eye movements. Real-time systems—with a low sampling frequency of 50/60 Hz—are used for clinical vestibular practice, but are generally considered not to be suited for measuring fast eye movements. In this paper, it is shown that saccadic eye movements, having an amplitude of at least 5°, can, in good approximation, be considered to be bandwidth limited up to a frequency of 25–30 Hz. Using the Nyquist theorem to reconstruct saccadic eye movement signals at higher temporal resolutions, it is shown that accurate values for saccade peak velocities, recorded at 50 Hz, can be obtained, but saccade peak accelerations and decelerations cannot. In conclusion, video eye trackers sampling at 50/60 Hz are appropriate for detecting the clinical relevant saccade peak velocities in contrast to what has been stated up till now.**

***Index Terms*—Eye movements, saccade, scleral search coil (SSC), video oculography (VOG).**

Manuscript received September 12, 2007; revised March 11, 2008. Current version published December 17, 2008. *Asterisk indicates corresponding author*.

R. Wierts was with the Faculty of Applied Physics, Eindhoven University of Technology, Eindhoven 5600 MB, The Netherlands. He is now with the Department of Nuclear Medicine and Molecular Imaging, University Medical Center Groningen, University of Groningen, Groningen 9700 RB, The Netherlands (e-mail: r.wierts@ngmb.umcg.nl).

*M. J. A. Janssen is with the Department of Biomedical Engineering, University Hospital Maastricht, Maastricht 6229 HX, The Netherlands, and also with the Department of ENT, Division of Balance Disorders, Maastricht University Medical Center, Maastricht 6229 HX, The Netherlands, and the Research Institute Brain and Behaviour, University Maastricht, Maastricht 6200 MD, The Netherlands (e-mail: m.janssen@mumc.nl).

H. Kingma is with the Department of Biomedical Engineering, Universtity Hospital Maastricht, Maastricht 6229 HX, The Netherlands, and also with the Department of ENT, Division of Balance Disorders, Maastricht University Medical Center, Maastricht 6229 HX, The Netherlands, the Research Institute Brain and Behaviour, University Maastricht, Maastricht 6200 MD, The Netherlands, and the Faculty of Biomedical Engineering, Eindhoven University of Technology, Eindhoven 5600 MB, The Netherlands (e-mail: herman.kingma@mumc.nl).

Digital Object Identifier 10.1109/TBME.2008.925290

I. Introduction

Since the development of small head-mounted video eye trackers, video oculography (VOG), has gained in popularity among clinical practitioners because of three dimensional recording of eye movements, low noise level, and high spatial accuracy. The developed head-mounted VOG systems can mainly be divided into two different groups: low-frequency sampling systems (50–60 Hz [1], [2]) operating real time and high-speed sampling systems up to 400 Hz [3]. Major drawbacks of the latter are that: 1) data are processed offline after the examination is completed—patient coaching during the examination is essential or 2) the available online systems are not useful in vestibular practice—they are unstable or uncomfortable during head movements. The drawback of real-time sampling VOG systems is the low sampling frequency, making measurement of fast eye movements problematic. Especially, for the calculation of saccadic peak velocities, an important parameter in clinical practice, high sampling frequencies, are always mentioned to be necessary. In a study of Juhola *et al.* [4], it was found that in order to obtain accurate values for the maximum eye velocity of a saccade of 20°, a sampling frequency of at least 300 Hz is required.

The purpose of this study is to evaluate saccade power spectra and evaluate a technique to improve the temporal resolution of 50 Hz eye movement recordings using VOG.

II. Methods

A. Eye Movement Recordings

Three healthy subjects without any history or evidence of ophthalmologic or neurologic disorders participated in the experiment. Ages ranged from 23 to 28 years. All subjects participated on a voluntary basis after giving their informed consent.

Subjects were seated in a chair. Movement of the head was minimized using a headrest attached to the chair. After calibration, subjects were asked to visually fixate a dot of 0.5 cm, projected on a screen positioned 1 m in front of the subjects. The dot moved abruptly from side to side, forcing the subjects to make horizontal midline-crossing saccades. The angle over which the spot moved started at a small value of 5° and increased in steps of 5° up to an angle of 25° (and 28°, limited by the dimensions of the screen). For each rotation angle, three saccades to the left and right were made, resulting in a total of 36 saccades per subject.

Since saccadic eye movements are the fastest eye movements one can make, they have the highest cutoff frequency of all eye movements. Thus, a sampling frequency, capable of accurately recording saccades, is also capable of recording all other types of eye movements.

Horizontal saccadic eye movements were recorded with the skalar scleral search coil (SSC) system S3020 (Skalar Medical). The SSC signal was amplified by an analogue amplifier having a bandwidth of 200 Hz. For the SSCs, the Skalar Medical combination annulus was used. The signal was recorded at a sampling frequency of 1 kHz.

B. Nyquist Sampling Theorem

When recording a dynamic signal, the used sampling frequency f_s is of high importance, since a too low sampling frequency results in a loss of information, called aliasing. The Nyquist critical frequency f_c equals half the sampling frequency f_s [5].

The Nyquist sampling theorem states that if a continuous function $x(t)$, sampled at a sampling interval $T_s = 1/f_s$, is bandwidth limited with a maximum frequency component, $f_{\max}$, equal to or smaller than f_c, then the function $x(t)$ is completely determined by its samples $x[n]$ and is given explicitly by

$$x(t) = \sum_{n=-\infty}^{+\infty} x[n] \frac{\sin[2\pi f_c (t - nT_s)]}{\pi (t - nT_s)} \quad (1)$$